Free Radical Biology and Medicine 101 (2016) 249–260

Contents lists available at ScienceDirect

Free Radical Biology and Medicine

journal homepage: www.elsevier.com/locate/freeradbiomed

PrxQ B from *Mycobacterium tuberculosis* is a monomeric, thioredoxin-dependent and highly efficient fatty acid hydroperoxide reductase

Aníbal M. Reyes[a,b], Diego S. Vazquez[c], Ari Zeida[d], Martín Hugo[a,b,1], M. Dolores Piñeyro[a,e], María Inés De Armas[a,b], Darío Estrin[d], Rafael Radi[a,b], Javier Santos[c], Madia Trujillo[a,b,*]

[a] *Departamento de Bioquímica, Facultad de Medicina, Universidad de la República, Montevideo, Uruguay*
[b] *Center for Free Radical and Biomedical Research, Universidad de la República, Montevideo, Uruguay*
[c] *Instituto de Química y Físicoquímica Biológicas "Prof. Alejandro C. Paladini" (IQUIFIB), Universidad de Buenos Aires and CONICET, Ciudad Autónoma de Buenos Aires, Argentina*
[d] *Departamento de Química Inorgánica, Analítica y Química-Física and INQUIMAE-CONICET, Facultad de Ciencias Exactas y Naturales, Universidad de Buenos Aires, Buenos Aires, Argentina*
[e] *Unidad de Biología Molecular-Institut Pasteur Montevideo, Montevideo, Uruguay*

ARTICLE INFO

Keywords:
Mycobacterium tuberculosis
Peroxiredoxin
Thioredoxin
Peroxynitrite
Fatty acid hydroperoxides
Thiol-dependent peroxidase
Peroxidatic and resolving cysteine

ABSTRACT

Mycobacterium tuberculosis (*M. tuberculosis*) is the intracellular bacterium responsible for tuberculosis disease (TD). Inside the phagosomes of activated macrophages, *M. tuberculosis* is exposed to cytotoxic hydroperoxides such as hydrogen peroxide, fatty acid hydroperoxides and peroxynitrite. Thus, the characterization of the bacterial antioxidant systems could facilitate novel drug developments. In this work, we characterized the product of the gene Rv1608c from *M. tuberculosis,* which according to sequence homology had been annotated as a putative peroxiredoxin of the peroxiredoxin Q subfamily (PrxQ B from *M. tuberculosis* or *Mt*PrxQ B). The protein has been reported to be essential for *M. tuberculosis* growth in cholesterol-rich medium. We demonstrated the *M. tuberculosis* thioredoxin B/C-dependent peroxidase activity of *Mt*PrxQ B, which acted as a two-cysteine peroxiredoxin that could function, although less efficiently, using a one-cysteine mechanism. Through steady-state and competition kinetic analysis, we proved that the net forward rate constant of *Mt*PrxQ B reaction was 3 orders of magnitude faster for fatty acid hydroperoxides than for hydrogen peroxide (3×10^6 *vs* 6×10^3 M^{-1} s^{-1}, respectively), while the rate constant of peroxynitrite reduction was $(0.6–1.4)\times10^6$ M^{-1} s^{-1} at pH 7.4. The enzyme lacked activity towards cholesterol hydroperoxides solubilized in sodium deoxycholate. Both thioredoxin B and C rapidly reduced the oxidized form of *Mt*PrxQ B, with rates constants of 0.5×10^6 and 1×10^6 M^{-1} s^{-1}, respectively. Our data indicated that *Mt*PrxQ B is monomeric in solution both under reduced and oxidized states. In spite of the similar hydrodynamic behavior the reduced and oxidized forms of the protein showed important structural differences that were reflected in the protein circular dichroism spectra.

1. Introduction

M. tuberculosis causes the death of million people per year all over the world (http://www.who.int/tb/publications/global_report/en/). Due to the emergence of multi- and extensively resistant strains to the drugs currently available for TD treatment, the identification of potential drug targets and the development of novel therapeutic approaches are a priority [1]. The bacterium is able to proliferate

Abbreviations: M. tuberculosis, *Mycobacterium tuberculosis*; TD, tuberculosis disease; Prx, peroxiredoxin; *Mt*PrxQ A, *M. tuberculosis* peroxiredoxin Q A; *Mt*PrxQ B, *M. tuberculosis* peroxiredoxin Q B; *Mt*Trx B and C, respectively, *M. tuberculosis* thioredoxin B and C; FF, Fully Folded; LU, Locally Unfolded; H_2O_2, Hydrogen Peroxide; 15-HpETE, 15S-hydroperoxy-5Z, 8Z, 11Z, 13E-eicosatetraenoic acid; *t*-bOOH, *tert*-butyl hydroperoxide; Cumene-OOH, cumene hydroperoxide; Cholesterol-OOH, a mixture of racemic 9- and 13- hydroperoxy octadeca-dienoic acid cholesteryl esters, cholesteryl linoleate hydroperoxide; HRP, Horseradish Peroxidase; DTNB, 5,5′-dithiobis-(2-nitrobenzoate); DTPA, Diethylenetriaminepentaacetic Acid; PMSF, Phenylmethylsulfonyl Fluoride; BHT, Butylated Hydroxytoluene; Xylenol Orange, 3,3'-Bis[N,N-bis(carboxymethyl)-aminomethyl]-o-cresolsulfonephthalein tetrasodium salt; CBA, Coumarin Boronic Acid; IPTG, Isopropyl-1-thio-β-d-galactopyranoside; DTT, Dithiothreitol; TCEP, Tris(2-carboxyethyl) phosphine; CD, Circular Dichroism; SEC, Size Exclusion Chromatography; FPLC, Fast Protein Liquid Chromatography; MD, Classical Molecular Dynamics; MALS, Multiangle Light Scattering; DMSO, Dimethyl Sulfoxide

* Corresponding author at: Departamento de Bioquímica, Facultad de Medicina, Universidad de la República, General Flores 2125, Montevideo 11800, Uruguay.
E-mail address: madiat@fmed.edu.uy (M. Trujillo).
[1] Present address: German Institute of Human Nutrition, University of Potsdam, Germany.

http://dx.doi.org/10.1016/j.freeradbiomed.2016.10.005
Received 20 June 2016; Received in revised form 16 September 2016; Accepted 6 October 2016
Available online 15 October 2016

inside the phagosomes of activated macrophages, its main host cells, where reactive oxygen and nitrogen species including the cytotoxic peroxides hydrogen peroxide (H_2O_2), fatty acid hydroperoxides (FA-OOH) and peroxynitrite are formed [2–5]. Thus, the knowledge of the bacterial antioxidant defenses that allow peroxide detoxification could provide clues related to the pathogenic mechanisms and virulence of *M. tuberculosis* that in turn facilitate the design of therapeutic strategies.

The battery of enzymes with peroxidase activity expressed in *M. tuberculosis* includes the heme-containing protein catalase-peroxidase, responsible for isoniazid activation, and a series of thiol-dependent peroxidases of the peroxiredoxin (Prx) family [6]. The latter are ubiquitous proteins that participate not only in peroxide detoxification but also in redox signaling [7] and display a bisubstratic ping-pong mechanism of catalysis [8]. Among them, the proteins encoded by the genes Rv2521 and Rv1608c are considered to be Prxs of the PrxQ subfamily (also referred as bacterioferritin comigratory proteins, Bcp) by sequence homology [9], but information regarding their catalytic activities is completely lacking. While the structure of *Mt*PrxQ A (Rv2521) is still unknown, the crystal structure of recombinant *Mt*PrxQ B[2] (Rv1608c) under reduced state has been recently reported at 1.35 Å resolution (PDBID: 5EPF). Evidences for the expression of both putative *Mt*PrxQs at a protein level exist, since they were detected both in the cytosolic and in the membrane-associated protein fractions (*Mt*PrxQ A) [11,12] or only in the membrane-associated protein fraction (*Mt*PrxQ B) of *M. tuberculosis* H37Rv strain [11,13,14]. *Mt*PrxQ B was reported to be essential for the growth of *M. tuberculosis* on cholesterol-rich media, which is an essential nutrient during animal chronic infections [15,16]. PrxQs usually behave as atypical two-cysteine Prxs, where the thiolate group at the peroxidatic cysteine residue (C_P-S^-) is oxidized by the peroxide substrate to form a sulfenate intermediate (C_P-SO^-) that reacts with the resolving cysteine (C_R) to form an intramolecular disulfide bridge. Disulfide formation in Prxs requires a not completely understood transition from a fully folded (FF) to a locally unfolded (LU) conformation that approaches C_P-SO^- to C_R allowing the disulfide to be formed [10]. The latter is then reduced by the reducing substrate, usually thioredoxin (Trx) [17]. In other cases, PrxQs lack C_R and the sulfenic acid formed in C_P is more efficiently reduced by glutathione/glutaredoxin system [18]. According to its sequence *Mt*PrxQ B would belong to the PrxQ subgroup that contains both C_P and C_R in helix α2, in a PXXX(T/S)XXC_PXXXXC_R motif that has been reported to suffer a striking conformational change in the transition from FF to LU, the latter one being trapped in the disulfide-containing oxidized form of the protein [10]. The oxidizing substrate specificity of the PrxQ subfamily is still unclear with some members catalyzing the reduction of a broad range of peroxides, including H_2O_2 and artificial organic hydroperoxides, with similar catalytic efficiency [19–21], whereas for some PrxQs, a preference for FA-OOH has been indicated [22–24], although kinetic data for their reduction are presently almost completely lacking. To note, *Xylella fastidiosa* PrxQ, a member of the PrxQ subfamily in which C_R is located in a different position (α3 helix), is the only PrxQ for which a peroxynitrite reductase activity has been demonstrated so far [19].

In this work, we measured for the first time the peroxidase activity of *Mt*PrxQ B. Through steady-state and pre-steady state kinetic analysis, we investigated the catalytic mechanisms as well as the preferential oxidizing and reducing substrates of this enzyme. We also established the hydrodynamic behavior of the protein under different redox states. Molecular dynamic simulations were performed to get insights into the molecular determinant of the changes in the structure of *Mt*PrxQ B that occurred upon oxidation.

[2] For the sake of clarity, we will use the term PrxQ instead of the less informative term Bcp to name the PrxQ/Bcp subfamily members as recently recommended (*10*) *Mt*PrxQ A and *Mt*PrxQ B have been previously referred as *Mt*Bcp and *Mt*Bcp B, respectively.

2. Materials and methods

2.1. Chemicals

Horseradish peroxidase (HRP), 5,5′-dithiobis-(2-nitrobenzoate) (DTNB), dithiothreitol (DTT), Tris(2-carboxyethyl) phosphine (TCEP), diethylenetriaminepentaacetic acid (DTPA), phenylmethylsulfonyl fluoride (PMSF), butylated hydroxytoluene (BHT), ferrous ammonium sulfate ($Fe(NH_4)_2(SO_4)_2$), *tert*-butyl hydroperoxide (*t*-bOOH) and cumene hydroperoxide (Cumene-OOH) were purchased from Sigma–Aldrich. *3,3'-Bis*[N,N-*bis(carboxymethyl)-aminomethyl*]-o-*cresolsulfonephthalein tetrasodium salt* (Xylenol Orange) was from AppliChem. Hydrogen peroxide (H_2O_2) was from Mallinckrodt Chemicals. 15S-hydroperoxy-5Z, 8Z, 11Z, 13E-eicosatetraenoic acid (15-HpETE) (purity ≥98%) and cholesteryl linoleate hydroperoxide (Cholesterol-OOH, a mixture of racemic 9- and 13- hydroperoxy octadeca-dienoic acid, cholesteryl esters) (purity ≥98%) was obtained from Cayman Chemicals. Coumarin boronic acid (CBA) was kindly supplied by Dr. Balaraman Kalyanaraman (Department of Biophysics and Free Radical Research Center, Medical College of Wisconsin, Milwaukee, USA). Stock CBA solutions were prepared in DMSO [25]. Isopropyl-1-thio-β-D-galactopyranoside (IPTG) was purchased from BioWorld. Peroxynitrite was synthesized from H_2O_2 and nitrous acid as described previously [26,27]. Treatment of stock solutions of peroxynitrite with granular manganese dioxide eliminated H_2O_2 remaining from the synthesis, and nitrite contamination was typically less than 30% of peroxynitrite concentration [28]. Fresh stock solutions of Cholesterol-OOH (120 μm) were solubilized by 2–3 h incubation in sodium phosphate (100 mM) buffer plus DTPA (0.1 mM) and sodium deoxycholate (20 mM), pH 7.4 and 25 °C [29]. Complete solubilization was tested by following absorption decrease at 600 nm.

All reactions described herein took place in sodium phosphate (100 mM) buffer plus DTPA (0.1 mM), pH 7.4 and 25 °C, unless otherwise indicated. Kinetic determinations were performed using an Applied Photophysics SX-20 stopped-flow spectrofluorimeter (mixing time < 1.2 ms).

2.2. Protein expression and purification

The gene for *Mt*PrxQ B (Rv1608c) in the expression vector pDEST17 was obtained from Dr. Ahmed Haouz, Institut Pasteur Paris, and was expressed as a recombinant His-tagged protein in *E. coli* BL21(DE3)pLysS strain. Sequence analysis indicated that the gene had a nucleotide substitution resulting in a protein with a point mutation from Ala93 to Thr. This substitution is frequent in PrxQ B from other non-pathogenic as well as pathogenic Mycobacteria, and found for example in PrxQ B from *M. indicus pranii*, *M. haemophilum*, *M. intracellulare* and *M. avium*, among others, which otherwise share > 85% sequence identity with *Mt*PrxQ B protein. Bacteria were grown at 37 °C in LB medium containing ampicillin (100 μg mL^{-1}) and chloramphenicol (30 μg mL^{-1}) until the optical density at 600 nm reached ~ 0.9 AU, and were then induced with IPTG (0.8 mM) for 4 h at 37 °C. After centrifugation at 4000 rpm during 30 min at 4 °C, the bacterial pellet was resuspended in Tris–HCl (20 mM), NaCl (500 mM) buffer pH 7.6 plus PMSF (1 mM) and disrupted by sonication. The protein was purified from the supernatant by affinity chromatography using a Nickel-charged column (HiTrap Chelating® GE Healthcare) and treated with DTT (2 mM) immediately afterwards, to reduce the protein which we found is otherwise prone to precipitation. Remaining imidazol and DTT were removed by gel filtration using HiTrap desalting columns (Amersham Bioscience) equilibrated with sodium phosphate (50 mM) buffer plus NaCl (100 mM) pH 7.4 using UV–VIS detection at 280 nm. Glycerol (10%) is then added to the protein which is afterwards stored at −80 °C. *Mt*PrxQ B C44S and C49S mutated versions of *Mt*PrxQ B were purchased from GenScript in expression vector pDEST17 and proteins expression and purification

followed the same procedure as for the wild type protein described above. The genes for expression of recombinant thioredoxin B and C from *M. tuberculosis* (*Mt*Trx B and *Mt*Trx C, respectively) in expression vector pET22b were kindly supplied by Dr. Marcelo Comini (Institut Pasteur Montevideo, Uruguay) and Dr. Leopold Flohé (Department of Chemistry, University of Padova, Italy and Departamento de Bioquímica, Facultad de Medicina, Universidad de la República, Uruguay), expressed in *E. coli* BL21 Star (DE3) strain as recombinant His-tagged proteins and purified as previously described [30].

2.3. Determination of peroxide concentration

The concentration of H_2O_2 in stock solutions was measured at 240 nm (ε_{240} =43.6 M^{-1} cm^{-1}) [31]. Peroxynitrite concentration was determined at alkaline pH at 302 nm (ε_{302} =1,670 M^{-1} cm^{-1}) [27]. Concentrations of other peroxides were calculated considering the purity of stock solutions (which were ≥98% pure in all cases) and verified by FOX assays using H_2O_2-calibration curves. To note, the ε value of FOX assays have small dependence on the structure of the particular hydroperoxide [32].

2.4. Determination of protein and thiol concentration

*Mt*PrxQ B, *Mt*Trx C and *Mt*Trx B concentrations were determined spectrophotometrically, using molar absorption coefficients at 280 nm of 7,450, 11,000 and 14,105 M^{-1} cm^{-1}, respectively, that were calculated according to their protein sequence [33]. Protein thiol contents were 2 thiols per protein for each enzyme as measured by the Ellman's assay (ε_{412} =14,150 M^{-1} cm^{-1}) [34]. The concentration of HRP was determined by its absorption at the Soret band (ε_{403} =1.02×10^5 M^{-1} cm^{-1} [35]).

2.5. Protein thiol reduction and oxidation

In some experiments, *Mt*PrxQ B was reduced immediately before use by incubation with excess DTT (2 mM) or TCEP (2 mM) for 30 min at 4 °C. The same procedure was used for *Mt*Trx C and *Mt*Trx B reduction. Excess reducing agents were removed by gel filtration using HiTrap Desalting® columns (GE Helthcare) and UV–VIS detection at 280 nm unless otherwise indicated. In other experiments, oxidized *Mt*PrxQ B was produced by treatment of reduced *Mt*PrxQ B with equimolar amounts of H_2O_2.

2.6. Peroxidase activity of MtPrxQ B

The peroxidase activity of wild type, C44S and C49S *Mt*PrxQ B using homologous *Mt*Trx B or C as reducing substrates and different hydroperoxides as oxidizing substrates were investigated taking advantage of the important decrease in intrinsic fluorescence intensity that occurs upon Trx oxidation as previously described [36,37], using an Aminco Bowman Series 2 luminescence fluorimeter (λ_{exc} =295 nm, λ_{em} =335 nm) or a stopped flow spectrofluorimeter (λ_{exc} =295 nm, total emission). The contribution to the total fluorescence changes from *Mt*PrxQ B fluorescence is negligible, due to the lack of tryptophan residues in *Mt*PrxQ B sequence which is otherwise used in catalytic amounts. The peroxidatic activity of *Mt*PrxQ B was also determined by following H_2O_2 or Cholesterol-OOH consumption using the FOX assay [32]. Briefly, DTT (2 mM) and *Mt*Trx C (10 μM) or *Mt*PrxQ B (2 μM) were incubated with H_2O_2 or Cholesterol-OOH solubilized in sodium deoxycholate (50 μM) in sodium phosphate (50 mM) buffer, pH 7.4, 25 °C. Aliquots (100 μl) were taken every 30 s and mixed with 900 μl of the FOX reagent and further incubated for 30 min at room temperature before absorbance measurement at 560 nm [38]. For measuring H_2O_2 consumption by *Mt*PrxQ B under non-catalytic conditions, reduced enzyme (20 μM) was mixed with H_2O_2 (50 μM) and the concentrations of the latter at indicated time points were also measured by the FOX assay. The extinction coefficient for H_2O_2 using this assay was determined (59,620 M^{-1} cm^{-1}) and was in close agreement with previously reported values [39].

2.7. Oxidizing substrate specificity of MtPrxQ B

The oxidizing substrate specificity of *Mt*PrxQ B was assessed using different potential substrates through steady-state as well as single turnover approaches.

Steady-state kinetic analysis of the peroxidase activity of MtPrxQ B. Kinetic analysis of the catalytic activity of *Mt*PrxQ B varying both *Mt*Trx C and the hydroperoxide substrate (H_2O_2 or 15-HpETE) concentrations were performed by following the decrease in intrinsic fluorescence intensity accompanying Trx oxidation in a stopped-flow spectrofluorimeter. The use of this equipment allowed to measure real initial rates of reactions, before any decrease in enzymatic activity due to potential oxidative inactivation occurred. *Mt*PrxQ B (0.5 μM) and the indicated concentrations of reduced *Mt*Trx C in one syringe were rapidly mixed with different concentrations of hydroperoxide present in the second syringe. After mixing, the rates of reaction were measured by monitoring the change in intrinsic fluorescence of *Mt*Trx C as it is oxidized (λ_{exc} =295 nm, total emission). Initial rates for the fluorescence changes at each *Mt*Trx C concentration were converted to rates of peroxide consumption (μM peroxide reduced per second per μM *Mt*PrxQ B) using Eq. (1) as previously described [21,40]. In the case of 15-HpETE, concentrations were chosen so as not to exceed critical micelle concentrations reported for arachidonic acid [41].

$$\text{Rate } (\mu M \text{ ROOH } s^{-1}\ \mu M^{-1} \textit{Mt}\text{PrxQ B}) = \text{Rate } (V\ s^{-1}).\ \frac{[\textit{Mt}\text{TrxC}]\mu M}{\Delta F\,(V).\ [\textit{Mt}\text{PrxQ B}]\mu M} \quad (1)$$

where [*Mt*Trx C] and [*Mt*PrxQ B] are the concentrations of the proteins in the assay, and ΔF is the change in fluorescence signal (in V) in the presence of excess peroxide for the same reductant concentration as that being analyzed. The initial rate of fluorescence decrease was determined by linear fitting of the experimental data during the first 2 s of the reactions. The initial velocity data was fitted to Daltziel equation

$$\frac{[\textit{Mt}\text{PrxQ B}]}{V_0} = \phi_0 + \frac{\phi_1}{[\text{ROOH}]} + \frac{\phi_2}{[\textit{Mt}\text{Trx C}]} + \frac{\phi_{1,2}}{([\text{ROOH}].\ [\textit{Mt}\text{Trx C}])} \quad (2)$$

and the coefficients ϕ were obtained from Daltziel plots of [*Mt*PrxQ B]/V_0 *vs* [ROOH] at different fixed concentrations of Trx. In the case of ping-pong mechanism, where no ternary complex is formed, $\phi_{1,2}$ is zero, so the primary plot gives parallel straight lines with slopes =ϕ_1 and intercepts =ϕ_0 +ϕ_2/[*Mt*Trx C]. ϕ_0 is the reciprocal value of k_{cat}, and ϕ_1 and ϕ_2 are the reciprocal values of the net forward rate constants of the reaction of the enzyme with ROOH (k_{ROOH}') and with Trx (k_{Trx}'), respectively [8,42]. From the primary Daltziel plot, we obtained ϕ_1. In terms of microscopic rate constants, ϕ_1 =(k_{-1} + k_2) /(k_1 . k_2)

$$\text{ROOH} + \textit{Mt}\text{PrxQ B-S}^- \underset{k_{-1}}{\overset{k_1}{\rightleftarrows}} [\textit{Mt}\text{PrxQ B-ROOH}] \underset{k_{-2}}{\overset{k_2}{\rightleftarrows}} \text{ROH} + \textit{Mt}\text{PrxQ B-SO}^-$$

ϕ_1 approaches the reciprocal value of the microscopic rate constant k_1 when the k_{-1} value of the backwards reaction is small compared with k_2.

Single turnover approaches to investigate peroxynitrite reduction by MtPrxQ B. The ability of *Mt*PrxQ B to reduce peroxynitrite was determined using both direct and indirect (competition) approaches.

a. Direct approach. Peroxynitrite decomposition at 310 nm was followed in the absence or presence of reduced *Mt*PrxQ B (16 μM) in a stopped-flow spectrofluorimeter [43]. The rate constant of the reaction

was calculated from initial rates of peroxynitrite decay as previously [44].

b. Competition approaches. The second-order rate constant of the reaction between reduced *Mt*PrxQ B and peroxynitrite was determined by two competition assays. In the first one, HRP was used as an alternative target for peroxynitrite as described previously [44,45]. Briefly, peroxynitrite (1 μM)-mediated HRP (2 μM) oxidation to Compound I in the absence or presence of increasing reduced *Mt*PrxQ B concentrations was followed at 398 nm ($\Delta\varepsilon_{398}$ =4.2×10^4 M^{-1} cm^{-1} [46]). The rate constant of peroxynitrite-mediated HRP oxidation to Compound I was determined as 3×10^6 M^{-1} s^{-1} under the experimental conditions employed herein (data not shown) in agreement with previously published data [47]. The rate constant of peroxynitrite-mediated *Mt*PrxQ B oxidation was calculated from HRP-Compound I yield obtained at different *Mt*PrxQ B concentrations as previously [45,48,49].

In the second competition assay, peroxynitrite (0.2 μM)-mediated CBA (1 μM) oxidation to 7-hydroxycoumarin in the absence or presence of increasing concentrations of reduced *Mt*PrxQ B was followed (λ_{ex} =332 nm, total emission) [25,50]. Since we used a 5 fold excess concentration of the competing targets and the time courses of the reactions fitted to exponential curves, the rate constant of peroxynitrite reduction by *Mt*PrxQ B was obtained from the slope of the plot of observed rate constants of fluorescence change *versus* enzyme concentration.

2.8. MtTrx B and C as reducing substrates for MtPrxQ B

The second order rate constants of the reduction of *Mt*PrxQ B by *Mt*Trx C and by *Mt*Trx B were determined by a single turnover kinetic analysis. We mixed reduced *Mt*Trx C (0.8 μM) or *Mt*Trx B (0.4 μM) with increasing concentration of previously oxidized *Mt*PrxQ B using a stopped-flow spectrofluorimeter. Single exponential curves were fitted to the experimental data. The rates constants of *Mt*PrxQ B reduction was determined from the slope of the plot of the observed rate constants of fluorescence change of *Mt*Trx C or *Mt*Trx B as a function of oxidized *Mt*PrxQ B concentration [37].

2.9. Hydrodynamic behavior

The molecular weights of reduced or oxidized *Mt*PrxQ B in solution were determined by multiangle light scattering (MALS). Enzyme samples (1 mg mL^{-1}) were prepared in Tris–HCl (50 mM), NaCl (75 mM), pH 7.4 (equilibration buffer). Reduced enzyme samples contained TCEP (2 mM). Oxidized enzyme consisted in reduced *Mt*PrxQ B (desalted to eliminate excess TCEP) treated with equimolar concentrations of H_2O_2. The samples were centrifuged at 4 °C and 16,000 rpm before injection on a SEC-FPLC System using a Superose 12 column (GE Healthcare) coupled to UV (Jasco Corporation, Japan) and MALS (Wyatt Technology) module detectors. The system was equilibrated at room temperature. The flow rate was set to 0.3 mL min^{-1} and the injection volume was 100 μL. Data analysis was performed using the Astra 6.0 software (Wyatt Technology).

2.10. Circular dichroism spectroscopy

The ellipticity of reduced and oxidized *Mt*PrxQ B was evaluated using a JASCO-810 spectropolarimeter (Jasco Corporation, Japan) equipped with a Peltier temperature controller. Samples were prepared in Tris–HCl (50 mM), NaCl (75 mM), pH 7.4 in a final protein concentration of 10 and 50 μM for far-UV and near-UV, respectively. Spectra were recorded in the range of 200–250 and 240–340 nm using a 0.1 and 1 cm path-length cell, respectively. Data acquisition was carried out at 25 °C and at least five spectra were acquired at a speed scan of 50 nm min^{-1} using a time constant of 0.5 s, and averaged. Finally, a blank scan was properly smoothed and subtracted from the corresponding average spectrum and expressed to molar ellipticity as:

$$[\theta]\ (\mathrm{deg\ dmol^{-1}\,cm^{-2}}) = \frac{\theta}{[Mt\mathrm{PrxQ\ B}](M).l.\ p.\ 10} \quad (3)$$

where θ is the raw ellipticity, [*Mt*PxQ B] is the enzyme concentration, l is the path length cell in centimeters and p is the number of peptide bonds.

2.11. Classical molecular dynamics

Classical molecular dynamics (MD) of *Mt*PrxQ B were performed in both reduced (fully folded, FF) and oxidized (locally unfolded, LU) states. For the reduced state, the crystal structure of *Mt*PrxQ B (PDBID: 5EPF) was used as starting structure. Cys44 was assumed to be in the reactive, deprotonated form. The disulfide model was generated starting from the reduced structure and by homology modeling of the entire α2 helix, *i.e.* residues from 39 to 64, as it is the protein region which suffers the more significant changes upon oxidation [51]. The structure of oxidized α2 helix of *Aeropyrum pernix* PrxQ (PDBID: 2CX3) was used as the template, and the homology model was generated using the *Swiss-Model* package [52]. Both, reduced and oxidized models were considered as monomers, as indicated by the multiangle light scattering experiments performed herein (see below).

The same MD protocol was applied for every system. Briefly, the system was solvated using a default method, with an octahedral box of 12 Å in radius with TIP3P water molecules [53]. All used residue parameters correspond to the parm99 Amber force field [54]. All simulations were performed using periodic boundary conditions with a 10 Å cutoff and particle mesh Ewald (PME) summation method for treating the electrostatic interactions. The hydrogen bond lengths were kept at their equilibrium distance by using the SHAKE algorithm, while temperature and pressure were kept constant with a Langevin thermostat and barostat, respectively, as implemented in the AMBER12 program [54]. The system was optimized in 1000 steps (10 with steep gradient and the rest with conjugate gradient). Then, it was slowly heated from 0 K to 300 K for 20 ps at constant pressure, with Berendsen thermostat, and pressure was equilibrated at 1 bar for 5 ps. After these two steps, a 10 ns MD long simulation at constant temperature (300 K) and constant volume was performed. Unrestrained 100 ns long production MD at the NPT ensemble was performed. All dynamics visualizations and molecular drawings were performed with *VMD 1.9.1* [55].

3. Results

3.1. Thioredoxin-dependent peroxidase activity of MtPrxQ B

The intrinsic fluorescence intensity of reduced *Mt*Trx B (10 μM) was not affected by the addition of H_2O_2 (30 μM) as expected considering the previously reported slow reactivity between this oxidant and another bacterial (*E. coli*) Trx (k=1.05 M^{-1} s^{-1} at pH 7.4–7.6 and 37 °C [56]). Further addition of *Mt*PrxQ B (1 μM) produced a rapid decrease in intrinsic fluorescence intensity of *Mt*Trx B, indicating that *Mt*PrxQ B was able to catalyze the H_2O_2-dependent *Mt*Trx B oxidation, (Fig. S1 a)). *Mt*PrxQ B also catalyzed the oxidation of *Mt*Trx C (10 μM) by H_2O_2 (10 μM) (Fig. 1). In addition, we confirmed the consumption of H_2O_2 (50 μM) by *Mt*Trx B (10 μM) and DTT (2 mM) using the FOX assay [38]: while in the absence of *Mt*PrxQ B there was a slow reduction of H_2O_2 (~ 5 μM in the first minute), its rate increased in the presence of the Prx (30 μM in the first minute, Fig. S1 b)). Under non-catalytic conditions, reduced *Mt*PrxQ B (20 μM) caused a rapid (< 1 min) and stoichiometric consumption of H_2O_2 (data not shown). Addition of *Mt*PrxQ B did not cause a decrease in the fluorescence of *Mt*Trx C in the presence of solubilized Cholesterol-OOH (10 μM) (Fig. S1c)). To note, the addition of sodium

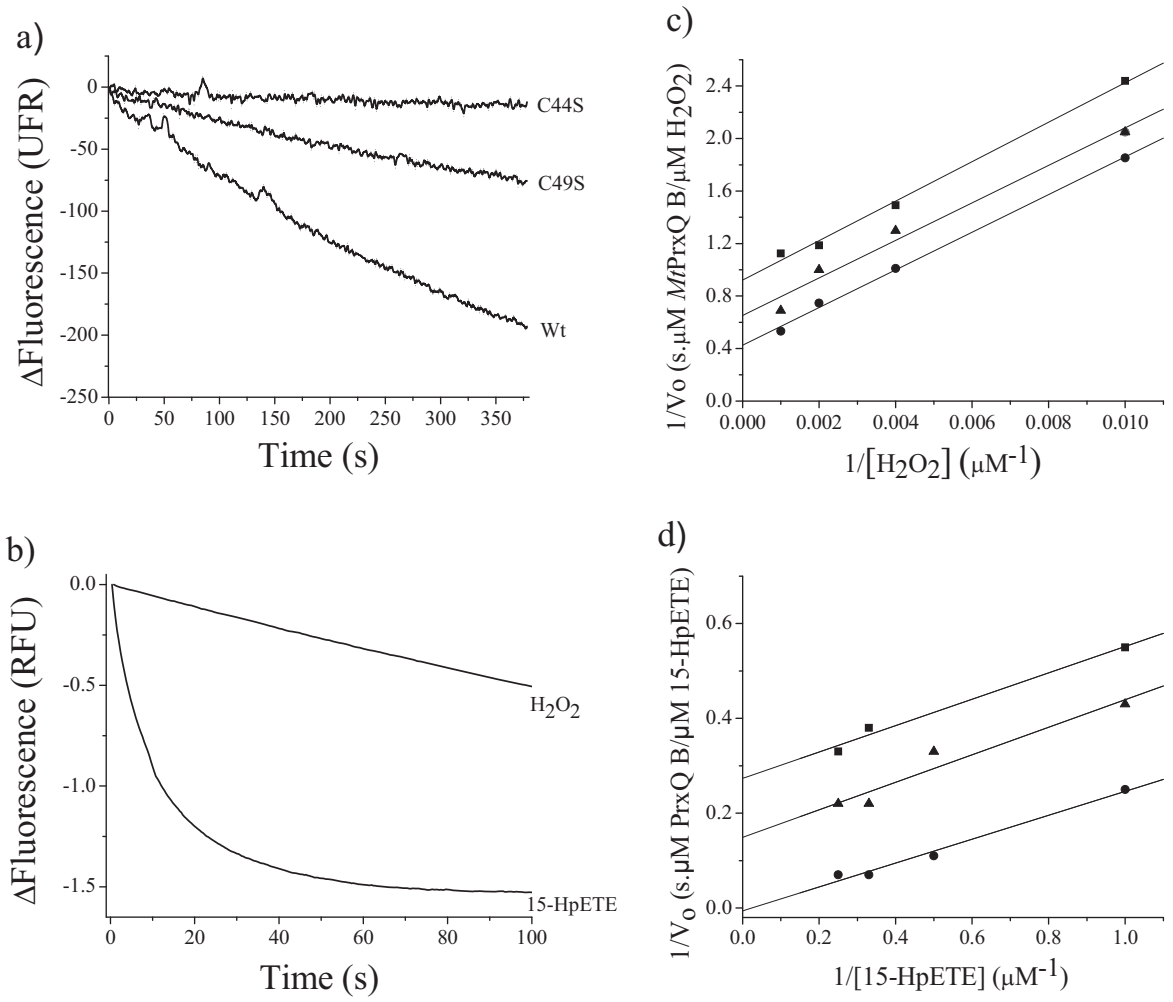

Fig. 1. Peroxidase activity of *Mt*PrxQ B and *Mt*PrxQ B Cys mutants C44S and C49S and steady-state kinetics analysis of H_2O_2 and 15-HpETE reduction by *Mt*PrxQ B a) Reduced *Mt*Trx C (10 μM) was mixed with H_2O_2 (10 μM) and exposed to Wild type (Wt), C44S or C49S *Mt*PrxQ B (0.2 μM) and time course of the intrinsic fluorescence change (λ_{ex} =295 nm, λ_{em} =335 nm) was recorded in an Aminco Bowman Series 2 fluorimeter. b) Time trace of total intrinsic fluorescence intensity (λ_{exc}=295 nm, total emission) of reduced *Mt*Trx C (10 μM) in the presence of *Mt*PrxQ B (0.5 μM) when rapidly mixed with H_2O_2 (10 μM) or 15-HpETE (10 μM) using a stopped flow spectrofluorimeter.c) Daltziel Plot of H_2O_2 reduction by *Mt*PrxQ B using *Mt*Trx C as reducing substrate. *Mt*Trx C (2.5 μM, squares; 7.5 μM, triangles; 10 μM circles) was incubated with different concentrations of H_2O_2 in the presence of *Mt*PrxQ B at pH 7.4 and 25 °C. Initial rate of the reactions were normalized by *Mt*PrxQ B concentration. d) Same analysis as in c) but using 15-HpETE as oxidizing substrate at different concentrations of *Mt*Trx C (2.5 μM, squares; 5 μM, triangles; 10 μM, circles).

deoxycholate at the same final concentration did not inactivate *Mt*PrxQ B when tested using H_2O_2 as oxidizing substrate (Fig. S1c) and d)). Accordingly, *Mt*PrxQ B did not increase the slow reduction of Cholesterol-OOH (50 μM) solubilized in sodium phosphate buffer (100 mM) plus sodium deoxycholate (10 mM) when it was incubated with DTT (2 mM) and *Mt*Trx C (10 μM) (Fig. S1 d)). Thus, solubilized Cholesterol-OOH is not a substrate of *Mt*PrxQ B. *Mt*PrxQ B (1 μM) catalyzed the oxidation of *Mt*Trx C (10 μM) by the artificial organic hydroperoxides *t*-bOOH and Cumene-OOH (10 μM) at rates that were 50% and 130%, respectively, compared with that of H_2O_2 (data not shown).

In order to determine whether *Mt*PrxQ B acts through a 1-Cys or 2-Cys mechanism, the peroxidase activities of single mutated forms of *Mt*PrxQ B in each of its two Cys residues were assayed. These two Cys are separated by four residues in the helix α2 and sequence homology analysis indicated that Cys44 and Cys49 would correspond to C_P and C_R, respectively (Fig. S2). Fig. 1a) shows no intrinsic fluorescence change of reduced *Mt*Trx C (10 μM) in the presence of *Mt*PrxQ B C44S and H_2O_2 (10 μM), indicating a completely lack of activity of this mutant, in agreement with the postulated role of Cys44 as C_P. *Mt*PrxQ B C49S showed ~60% lower activity compared with the wild type enzyme, consistent with the role of Cys49 as C_R which has a less crucial role in catalysis, as previously demonstrated for many other 2-Cys Prxs, including *E. coli* and *X. campestris* PrxQs [37,57,58]. Thus, in the absence of C_R, the C_P-SO^- can be reduced, although less efficiently, by alternative mechanisms also involving *Mt*Trx C as reducing substrate. These results are consistent with data indicating that members of the PrxQ subfamily can function also as 1-Cys Prxs [59,60].

3.2. Kinetics of MtPrxQ B oxidation

3.2.1. Oxidation by H_2O_2 and 15-HpETE

The time courses of total intrinsic fluorescence decrease (λ_{exc}=295 nm) that occur during *Mt*Trx C (10 μM) oxidation by H_2O_2 or 15-HpETE (10 μM) catalyzed by *Mt*PrxQ B (0.5 μM) are shown in Fig. 1b). The change in fluorescence intensity was much faster when 15-HpETE was used as oxidizing substrate compared to the same concentration of H_2O_2. A steady-state kinetic analysis using Daltziel equation (Eq. (2)) was performed to determine the catalytic efficiencies of *Mt*PrxQ B towards H_2O_2 or 15-HpETE. The slopes obtained from Daltziel plots using different concentrations of *Mt*Trx C were very similar (Fig. 1c) and d)), as expected for an enzyme with a ping-pong catalytic mechanism as was already described for this kind of enzymes [8]. From the reciprocal value of the slope of the linear fit of the data,

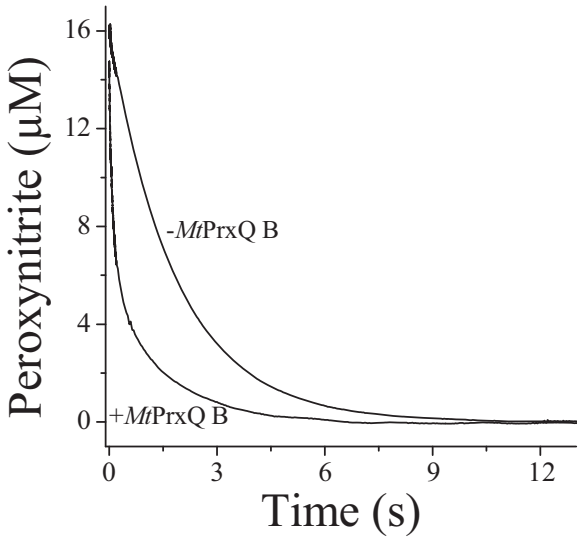

Fig. 2. Peroxynitrite reductase activity of *Mt*PrxQ B. Time trace of peroxynitrite decay in absence and presence of reduced *Mt*PrxQ B (16 μM) at pH 7.4 at 25 °C.

the net forward rate constants of the reduction of H_2O_2 and 15-HpETE by *Mt*PrxQ B were estimated as $(6.0 \pm 1.0) \times 10^3$ M^{-1} s^{-1} (Fig. 1c) and $(3.0 \pm 0.5) \times 10^6$ M^{-1} s^{-1} (Fig. 1d)), respectively, at pH 7.4 and 25 °C.

Accordingly, the reaction of *Mt*PrxQ B with H_2O_2 was not fast enough to compete with H_2O_2-mediated HRP oxidation to Compound I (k=2×10^7 M^{-1} s^{-1} [61]), even when a 17 fold higher concentration of *Mt*PrxQ B (17 μM) than HRP (1 μM) was used (data not shown). Due to limitations in concentrations of *Mt*Trx C that we could achieve, that precluded to repeat steady-state kinetic determinations at higher reducing substrate concentrations required to make secondary plots, the rest of the kinetic determinations performed herein made use of the ping-pong catalytic mechanism of *Mt*PrxQ B, which allowed us to analyze the oxidative and reductive parts of the catalytic cycle independently, using non-catalytic conditions.

3.2.2. Oxidation by peroxynitrite

In addition to H_2O_2 and FA-OOH, activated macrophages can form the unstable peroxide peroxynitrite whose protonated form (ONOOH) homolyses at physiological pH with a rate constant of 0.3 s^{-1} at pH 7.4 and 25 °C [62]. Peroxynitrite (17 μM) decay was accelerated in the presence of reduced *Mt*PrxQ B (16 μM) (Fig. 2), confirming its peroxynitrite reductase ability. The initial rate of peroxynitrite decay in the presence of reduced *Mt*PrxQ is given by:

$$V_0 = k.\ [\text{peroxynitrite}]_0.\ [Mt\text{PrxQ B}]_0 \quad (4)$$

From the linear fit of peroxynitrite decay in the presence of the enzyme during the first 20 ms and initial reactant concentrations employed, the rate constant of *Mt*PrxQ B oxidation by peroxynitrite was calculated as 5×10^5 M^{-1} s^{-1} at pH 7.4 and 25 °C. To note, there was no appreciable peroxynitrite decay in the absence of the enzyme during the same 20 ms period. The rate constant obtained is probably underestimated, since with the observed rate of peroxynitrite decay (127 μM s^{-1}) and even during the first 20 ms of reaction, initial concentrations of reactants would have decreased more than 10%. Thus, to better explore the kinetics of the reaction, we utilized competition approaches as described in Section 2.

In the first competition assay, *Mt*PrxQ B and HRP compete for peroxynitrite. Rapid mixing of HRP (2 μM) with peroxynitrite (1 μM) in the absence of *Mt*PrxQ B caused the stoichiometric formation of HRP-Compound I. In the presence of *Mt*PrxQ B, there was a decrease in the yields of HRP-Compound I formation (Fig. 3). Kinetic analysis of the data indicated that the second order rate constant of the reduction of peroxynitrite by *Mt*PrxQ B was of $(1.4 \pm 0.3) \times 10^6$ M^{-1} s^{-1} at pH 7.4 and 25 °C.

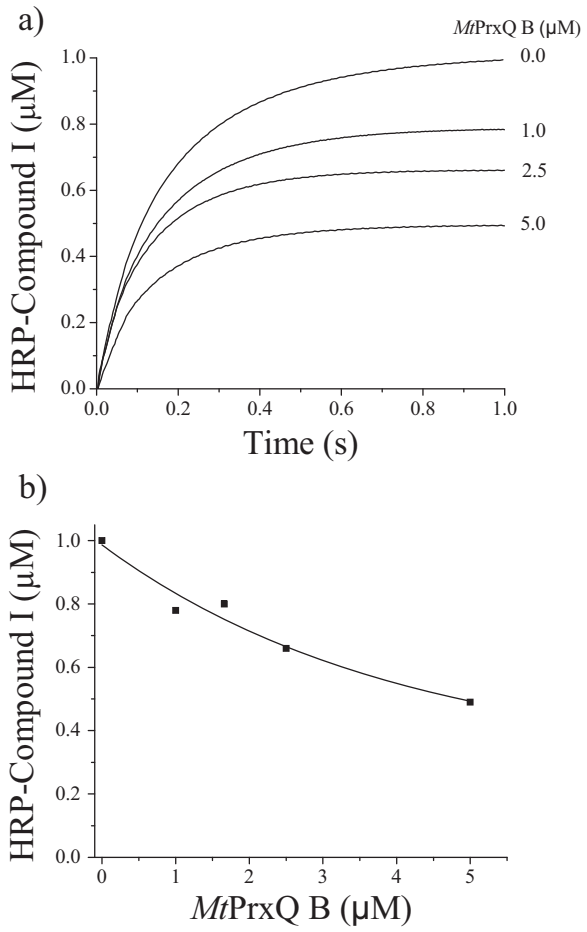

Fig. 3. Kinetics of peroxynitrite reduction by *Mt*PrxQ B. a) Time trace of the formation of Compound I caused by the oxidation of HRP (2 μM) by peroxynitrite (1 μM) and in the presence of increasing concentrations of *Mt*PrxQ B (0.0, 1.0, 1.5, 2.5, 5.0 μM) at pH 7.4 at 25 °C. b) HRP-Compound I concentration formed was plotted *versus* *Mt*PrxQ B concentration. The continuous line represents HRP-Compound I yields simulated according to a simple competition system using GEPASI program [79], a rate constant of HRP oxidation by peroxynitrite of 3×10^6 M^{-1} s^{-1} and the rate constant of *Mt*PrxQ B oxidation calculated herein (1.4×10^6 M^{-1} s^{-1}).

Additionally, CBA was used in competition with *Mt*PrxQ B for peroxynitrite. The presence of *Mt*PrxQ B decreases the formation of 7-hydroxycoumarin and increase the observed rate constant of CBA oxidation (Fig. 4). The slope of the plot of k_{obs} *vs* *Mt*PrxQ B concentration indicated that the second order rate constant for the reduction of peroxynitrite by *Mt*PrxQ B was $(6.6 \pm 0.1) \times 10^5$ M^{-1} s^{-1} at pH 7.4 and 25 °C. The y-intercept represented the observed rate constant of the reaction between peroxynitrite and CBA (1 μM) in the absence of *Mt*PrxQ B, indicating a rate constant of 1.8×10^6 M^{-1} s^{-1} which is similar to the previously reported value of $(1.1 \pm 0.2) \times 10^6$ M^{-1} s^{-1} at pH 7.4 and 25 °C [25].

3.3. Kinetics of MtPrxQ B reduction by MtTrx B and MtTrx C

The reducing substrates of 2-Cys PrxQs are usually thioredoxins, which can recycle the disulfide bond in the oxidized form of PrxQs at the expense of thioredoxin reductase/NADPH [19,21]. Incubation of reduced *Mt*Trx C with oxidized *Mt*PrxQ B in excess caused a rapid decrease in the intrinsic fluorescence intensity of the former. Experimental data was fitted to exponential curves, from which observed rate constants (k_{obs}) at different concentrations of *Mt*PrxQ B were obtained (Fig. 5). From the slope of the plot of k_{obs} *versus* *Mt*PrxQ B concentrations the rate constant for the reduction of

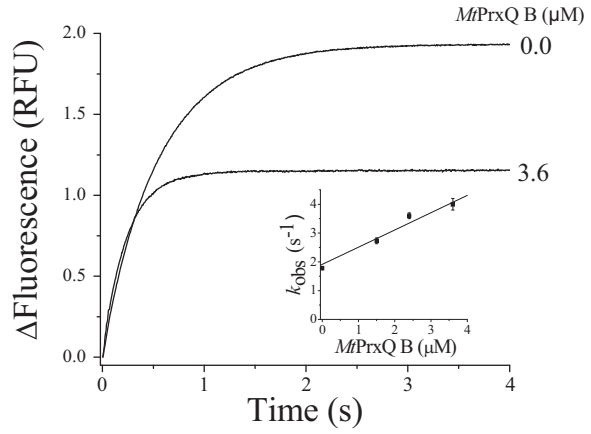

Fig. 4. Competition kinetic assay using CBA for the peroxynitrite reduction by *Mt*PrxQ B. Time courses of the formation of 7-hydroxycoumarin after mixing CBA (1 μM) and peroxynitrite (0.2 μM) in the absence or in the presence of reduced *Mt*PrxQ B (3.6 μM) at pH 7.4 at 25 °C. The inset shows a plot of the observed rate constants of 7-hydroxycoumarin formation plotted as a function of *Mt*PrxQ B concentration.

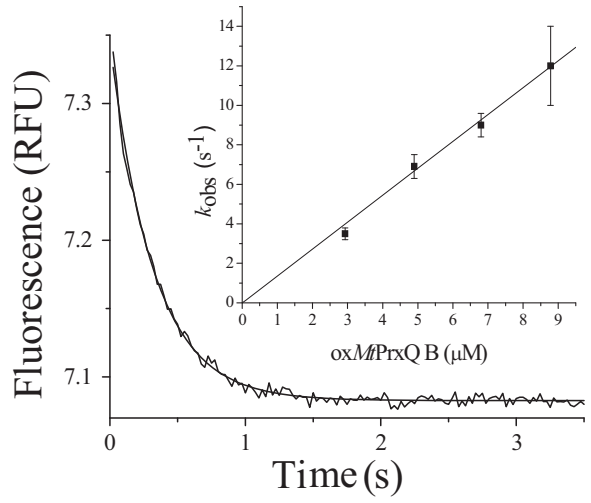

Fig. 5. Kinetics of *Mt*PrxQ reduction by *Mt*Trx C. Time trace of total intrinsic fluorescence intensity change (λ_{exc}=295 nm, total emission) of reduced *Mt*Trx C (0.8 μM) when mixed with oxidized *Mt*PrxQ B (2.9 μM) at pH 7.4 and 25 °C. Continuous line: experimental data; dashed line: fit to a single exponential curve. The inset shows the effect of *Mt*PrxQ B concentration on the observed rate constants of fluorescence change of *Mt*Trx C (0.8 μM).

oxidized *Mt*PrxQ B by *Mt*Trx C was determined as (1.0 ± 0.4) ×10^6 M^{-1} s^{-1} at pH 7.4 and 25 °C. In turn, *Mt*Trx B reduced *Mt*PrxQ B with a rate constant of (5.0 ± 0.1) ×10^5 M^{-1} s^{-1} at pH 7.4 and 25 °C (Fig. S3).

3.4. Influence of MtPrxQ B redox state in protein structure

3.4.1. Hydrodynamic behavior of reduced and oxidized MtPrxQ B in solution

Members of the PrxQ subfamily behave either as monomers or dimers in solution. The reported structure of reduced *Mt*PrxQ B indicated that it is monomeric in the crystal (PDBID: 5EPF) and so far, no data regarding the structure of the oxidized form of the enzyme has been reported. To determine the oligomeric state of reduced and oxidized *Mt*PrxQ B in solution, we performed MALS experiments . Fig. 6 shows the elution profiles of reduced (in the presence of TCEP (2 mM)) and oxidized *Mt*PrxQ B (50 μM). In both cases, the enzyme showed a similar elution profile and was predominantly monomeric as judged by the molecular mass of 16.8 ± 0.8 and 17.9 ± 1.6 kDa obtained for reduced and oxidized *Mt*PrxQ B, respectively, which is in agreement

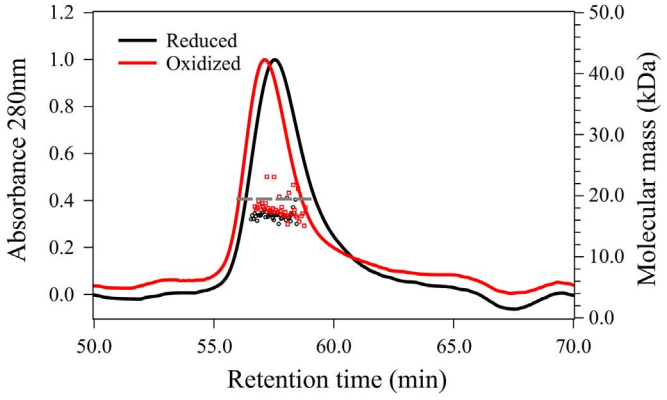

Fig. 6. Hydrodynamic behavior of reduced and oxidized *Mt*PrxQ B. Chromatograms of reduced (in the presence of TCEP 2 mM, black line) and oxidized (red line) *Mt*PrxQ B (48 μM) in buffer Tris–HCl (50 mM) plus NaCl (75 mM) pH 7.4 at 25 °C. Molecular mass determination by MALS of reduced and oxidized *Mt*PrxQ B are indicated by black circle and red square symbols, respectively. The dash gray line indicate the theoretical mass obtained by the sequence of 19470 Da. In both cases the flow rate was set at 0.3 mL min^{-1}. In the sake of clarity, only one of each 6 experimental point are shown, although all of them were considered to calculate the reported molecular mass. (For interpretation of the references to color in this figure legend, the reader is referred to the web version of this article.).

with the theoretical mass of 19470 Da per subunit obtained by sequence analysis. Moreover, the well-defined elution profile suggests a homogeneous conformational population in solution for both conditions, reflecting that the oxidation state do not alter neither the oligomeric state of the protein, as reported for other members of the Prx family [48,63] nor the global conformation of *Mt*PrxQ B.

3.4.2. Change in conformation during protein oxidation

To evaluate the conformational change associated with *Mt*PrxQ B oxidation, the far- and near-UV CD spectra of the reduced and oxidized forms of the protein were recorded (Fig. 7a) and b), respectively). Upon oxidation, the far-UV CD spectra of *Mt*PrxQ B showed a significant loss of the negative signal at 208 nm and a slightly shift of the negative band from 220 nm to 218 nm, which is compatible with a gain of random coil signal [64] and supported by the shape of the differential spectrum that results from the subtraction between the corresponding ones to the reduced and oxidized states (Fig. 7a), blue dashed line (d)). Data was too noisy at λ < 200 nm precluding the analysis of that region of the far CD spectra (Fig. 7a)), and precise content of secundary structures in the reduced and oxidized protein samples could not be calculated. Overall, the observed changes in the far UV CD spectra are compatible with previous data indicating that a partial unfolding of α2 helix occurs during FF to LU transition of PrxQs with C_R in α2 helix [10] which was evident when comparing the molecular dynamic simulations of the reduced and oxidized forms of the protein (Fig. 4S). Furthermore, in the near-UV CD spectra, the loss of the aromatic signals at 268, 278 and 285 nm evidences changes in the environment of aromatic residues (Phe and Tyr) upon oxidation (Fig. 7b)). Reductants were able to reverse these changes, as shown in the green solid line (c) of Fig. 7a) and b), for the far- and near-UV CD spectra, respectively.

In order to gain an atomistic detailed insight about this conformational change, we performed extensive MD simulations of both oxidation states of the enzyme. The superposition of representative structures from both states is presented in Fig. 8a). The conformational change accompanying *Mt*PrxQ B oxidation determined the exposure of several amino acids, including both Cys residues, to establish a tongue-shaped loop facing outwards the protein core (see Fig. 8a)). Certainly, the microenvironment surrounding both Cys, is pretty much distorted. Among these changes, it is worth to notice that a series of aromatic residues in the proximity of the active site, suffered important side chain conformational rotations, which led to an important solvent

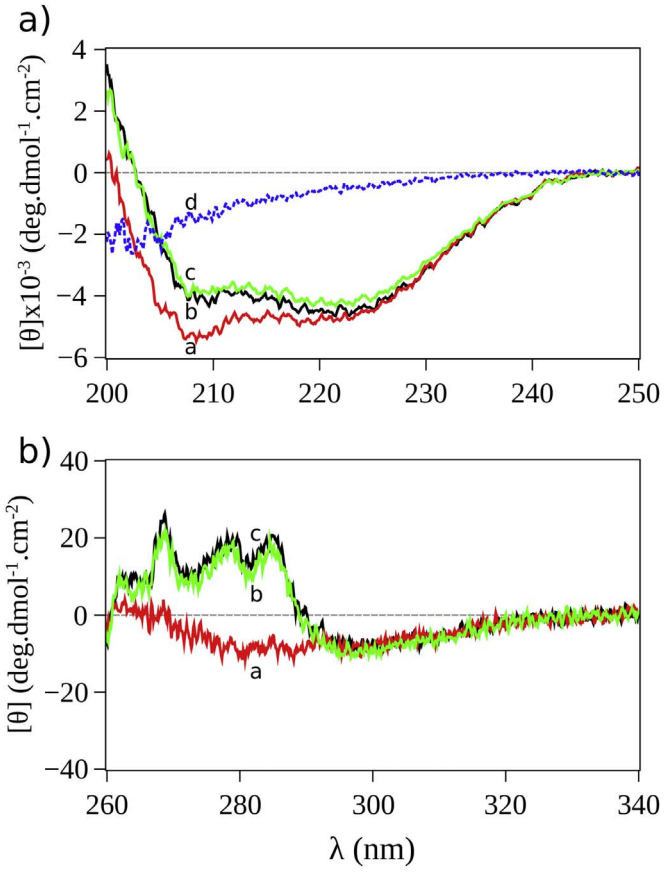

Fig. 7. *Mt*PrxQ B structural changes of upon oxidation. Far a) and Near b) UV CD spectrum of reduced (in the presence of TCEP 1 mM, black line, (a) and oxidized (, red line, (b)) *Mt*PrxQ B in buffer Tris-HCl (50 mM) plus NaCl (75 mM) pH 7.4 and 25 °C. The post-oxidation addition of excess of TCEP to oxidized enzyme is also shown (green line, (c)). In addition, the differential spectrum between the reduced and oxidized states is shown (blue dash line, (d)) which is compatible with a random coil structure. Protein concentrations used were 10 μM a) and 50 μM b) (For interpretation of the references to color in this figure legend, the reader is referred to the web version of this article.).

exposure increase (see Fig. 8b) and 8c). This effect was quantified by calculating the solvent accessible surface area (SASA) for these selected aromatic residues from the whole simulation, showing a significant increase of this property value upon enzyme oxidation (Fig. 8d)). Particularly, the main effect can be explained broadly by looking only at Phe51, Tyr36 and Tyr87, which are the amino acids that showed the major changes. The modification in the aromatic residues microenvironment is in perfect agreement with the near-UV CD spectra changes that were presented above (see Fig. 7b).

4. Discussion

In *M. tuberculosis* databases, *Mt*PrxQ B is annotated as a putative Prx of the PrxQ/BCP subfamily, but experimental evidence for the peroxidase function of the protein was lacking so far (http://genome.tbdb.org; http://tuberculist.epfl.ch). Data shown in Fig. 1 demonstrated the peroxidase activity of recombinant *Mt*PrxQ B. As expected according to sequence homology, it acted as a 2-Cys Prx, Cys44 being C_P, which is completely essential for activity, whereas Cys49 acted as C_R, and as for many other 2-Cys Prxs, the catalytic activity importantly decreased but was not completely lost in its absence [18,37].

*Mt*PrxQ B was able to reduce a broad spectrum of natural hydroperoxides including H_2O_2, FA-OOH (Fig. 1), *t*-bOOH, Cumene-OOH and peroxynitrite (Figs. 2–4), but kinetic measurements indicated a preference for FA-OOH followed by peroxynitrite, while reduction of H_2O_2 was much slower (Table 1). The enzyme did not reduce cholesterol-OOH (Fig. S1c) y d)). Reduction of H_2O_2 by *Mt*PrxQ B was equally rapid or ~ 10 fold slower than by other members of the PrxQ subfamily, with the exception of *Xf*PrxQ when measured by competition with HRP which was surprisingly fast [19]. In our hands, *Mt*PrxQ B did not inhibit HRP oxidation by H_2O_2, in agreement with the rate constant determined herein for the former reaction by steady-state kinetics (Fig. 1c)) which was ~ 10^3 slower than for HRP (6×10^3 *vs* 2×10^7 M^{-1} s^{-1} [61]). Regarding peroxynitrite, *Mt*PrxQ B was as reactive as *Xf*PrxQ, the only other PrxQ protein whose reactivity with this oxidant has been determined so far [19]. To note, although several reports indicated that PrxQs are not especially reactive towards artificial organic hydroperoxides (*t*-bOOH and Cumene-OOH) a preference for FA-OOH had already been indicated for several members of the subfamily, although reported rate constant values are scarce (Table 1). Indeed, by analyzing the crystal structures of different oxidizing states of PrxQ from *Xanthomonas campestris* (which belongs to the subgroup of PrxQs with C_R in α3 hélix) and co-cristalized molecules Liao et al. proposed a model for interactions of a hydrophobic pocket of the enzyme with the alkyl chains of hydroperoxides of 16 (or more) carbon atoms [58]. Like *Mt*PrxQ B, *Xc*PrxQ react at similar rates with Cumene-OOH and H_2O_2, ~3×10^4 M^{-1} s^{-1}, [65]. Unluckily, the reaction of *Xc*PrxQ with FA-OOHs was not investigated. Overall, the scarcity of kinetic data precluded to establish a relationship between structural properties of PrxQs (for instance, abscence/presence and localization of C_R) and substrate specificity at this point (Table 1).

According to kinetic data, and considering that *M. tuberculosis* expresses many other peroxidases able to reduce H_2O_2 and peroxynitrite much faster than *Mt*PrxQ B (Table 2) we suggest that the main function of the protein would be the reduction of FA-OOH. To note, *M. tuberculosis* lacks organic hydroperoxide reductase (OHR), which is responsible for organic hydroperoxides reduction in many other bacteria [66,67], and among the other Prxs expressed in *M. tuberculosis*, only *Mt*AhpE has been reported to reduce these FA-OOH at extremely high rates (~10^8 M^{-1} s^{-1}), which has been associated with the presence of a superficial hydrophobic grove close to C_P that favors positioning these substrates in a reactive conformation [38,68]. On the contrary, *Mt*AhpC showed lower catalytic activity with FA-OOH than with H_2O_2, and *Mt*Tpx was not active at all using FA-OOH as substrate [30]. Thus, *M. tuberculosis* expresses a battery of antioxidant enzymes whose oxidizing substrate specificity only partially overlaps, and specialization toward a particular kind of hydroperoxide could help to rationalize the expression of different members of the Prx family in the bacteria.

With respect to the reducing substrate, 2-Cys members of the PrxQ subfamily are usually more efficiently reduced by homologous Trxs. Exceptions are the Bcps of *Sulfolobus solfataricus* that are reduced by a member of the PDI family [69,70]. Both *Mt*Trx B and C rapidly reduced oxidized *Mt*PrxQ B, with rate constants in the order of 10^5–10^6 M^{-1} s^{-1} (Figs. 5 and 3S), thus providing a route for efficient enzyme recycling at the expense of thioredoxin reductase/NADPH.

MALS studies of reduced *Mt*PrxQ B indicated that it is mostly a monomeric protein in solution, with a mass ~17 kDa that is close to the theoretical calculated molecular mass (Fig. 6). This result is in agreement with the crystal structure of reduced *Mt*PrxQ B that was recently resolved by Abendroth, J. et al. with high resolution (1.35 Å) (PDBID: 5EPF). Members of the PrxQ subfamily of Prxs are either monomeric or A-type dimeric proteins. A detailed description of the structural characteristics of dimeric PrxQs showed that the dimeric A-type interface is stabilized mostly by interactions involving ~30 residues that have been previously grouped into regions 0 – 4 [10]. The buried area is mostly nonpolar and several aromatic residues that largely contribute to the interface (Phe 45, Trp79, Tyr98, in *Ap*PrxQ sequence) are well conserved among dimeric PrxQs but not in *Mt*PrxQ B as well as other monomeric PrxQs (Fig. S2). To note, Trp79 is

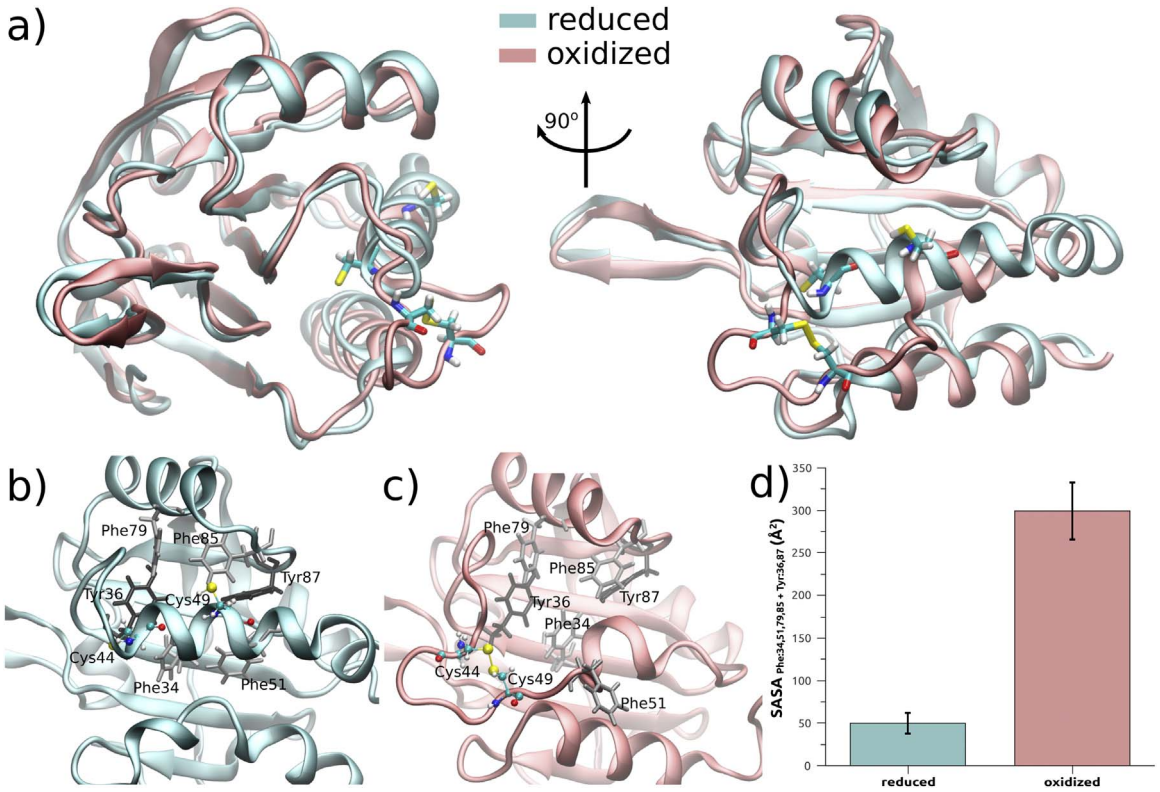

Fig. 8. Structure changes of *Mt*PrxQ B upon oxidation. a) Structural superposition of representative structures of reduced (cyan) and disulfide (magenta) states of *Mt*PrxQ B obtained by MD simulations. b) and c) Close view of the active site and the microenvironment surrounding the catalytic Cys residues. Aromatic residues (Phe and Tyr) are highlighted. d) Solvent accessible surface area (SASA) of Phe and Tyr residues nearby the active site, calculated from MDs. Average and standard deviations correspond to the sum of SASA from Phe34, Tyr36, Phe51, Phe79, Phe85 and Tyr87.

Table 1
Oxidizing substrate specificity of members of the PrxQ subfamily.

PrxQ	k_{H2O2} (M^{-1} s^{-1})	$k_{t\text{-bOOH}}$ (M^{-1} s^{-1})	$k_{Cumene\text{-}OOH}$ (M^{-1} s^{-1})	$k_{FA\text{-}OOH}$ (M^{-1} s^{-1})	$k_{peroxynitrite}$ (M^{-1} s^{-1})	Refs.
*Mt*PrxQ B	6×10^3 [a]	ND [b]	ND [b]	3×10^6 [a]	1.4×10^6 [c] 6.6×10^5 [d]	Herein
*Ec*PrxQ [e]	1.6×10^4	2.3×10^2	1.2×10^4	ND	ND	[21]
*Ec*PrxQ [f]	2.45×10^3	8.5×10^2	ND	1.2×10^4	ND	[24]
*Pt*PrxQ [g]	8×10^3	2.4×10^3	2.4×10^4	ND	ND	[20]
*At*PrxQ [h]	≫1	1	> 1	< 1	ND	[73]
Anasp PrxQ 1 and 3 [i]	> 1	1	≫1	⋙1	ND	[22]
*Xf*PrxQ	3.4×10^4 [j] 4.5×10^7 [k]	5.6×10^3 [j]	5.3×10^4 [j]	ND	1.04×10^6 [k]	[19]
*Rs*PrxQ [l]	3.3×10^4	ND	3.3×10^4	ND	ND	[59]
*Hp*PrxQ [m]	1	1	ND	>	ND	[23]
*Xc*PrxQ [a]	3×10^4	ND	3×10^4	ND	ND	[65]

Abbreviations: *Mt=Mycobacterium tuberculosis*; *Ec=Escherichia coli*; *Pt=Populus trichocarpa*; *At=Arabidopsis thaliana*; *Anasp=Anabaena sp.*; *Xf=Xylella fastidiosa*; *Rs=Rhodobacter sphaeroides*; *Hp=Helicobacter pylori*; *Xc=Xanthomonas campestris*.
The symbols > 1, > > 1 and > > > 1 indicate increaing higher activities compared with t-bOOH, taken as a reference, and indicated as 1. The symbol < 1 indicate lower activity than with t-bOOH.

[a] From steady state kinetic analysis at pH 7.4 and 25 °C.

[b] Although the rate constant of *Mt*PrxQ B oxidation by *t*-bOOH and Cumene-OOH were not determined, the enzyme was active with both substrate and the rates were 50% and 130%, respectively, compared with that of H_2O_2.

[c] competition with HRP at 7.4 and 25 °C.

[d] competition with CBA at pH 7.4 and 25 °C;

[e] k_{cat}/Km values, calculated from apparent Km and k_{cat} values obtained at 10 μM Trx, pH 7 and 25 °C.

[f] calculated from apparent Km and k_{cat} values obtained using 0.8 μM Trx, pH 7 and 25 °C.

[g] pH 7.

[h] higher peroxidase activity towards H_2O_2, followed by Cumene-OOH, *t*-bOOH (the latter is shown as 1 only for comparative purposes) and less active towards FA-OOH reduction. Activity was measured by hydroperoxide consumption by the FOX assay.

[i] higher peroxidase activity toward FA-OOH followed by Cumene-OOH, H_2O_2 and *t*-bOOH (the latter is shown as 1 only for comparative purposes), measured from hydroperoxide consumption using the FOX assay, at pH 7.4, 37 °C.

[j] k_{cat}/Km values at pH 7.4 and 37 °C.

[k] competition with HRP at pH 7.4 and 37 °C.

[l] k_{cat}/Km values, calculated from apparent Km and k_{cat} values obtained at 20 μM Trx, pH 7.3 and 25 °C.

[m] higher peroxidase activity toward FA-OOH compared with H_2O_2 or *t*-bOOH (shown as 1 only for comparative purposes), measured following NADPH consumption using a coupled assay at pH 7.

Table 2
Reactivity of Prxs from *M. tuberculosis*

*Mt*Prx	Prx subfamily	Proposed main oxidizing substrates	Reducing substrate	References
AhpC (Rv2428)	AhpC/Prx1,	H_2O_2 (k=3.7×10^7 M^{-1} s^{-1})[a] peroxynitrite (k=1.6×10^6 M^{-1} s^{-1})	*Mt*AhpD, *Mt*TrxC	[74,75,30,76]
Tpx (Rv1932)	Tpx,	peroxynitrite (k=1.33×10^7 M^{-1} s^{-1})	*Mt*TrxB, *Mt*TrxC	[37]
AhpE (Rv2238c)	AhpE,	peroxynitrite (k=1.9×10^7 M^{-1} s^{-1}) FA-OOH (k ~ 10^8 M^{-1} s^{-1})	*Mt*Mrx 1 ± mycothiol[b]	[38,49,77]
PrxQ B (Rv1608c)	PrxQ/Bcp	FA-OOH ($k_{15\text{-HpETE}}$=3×10^6 M^{-1} s^{-1}) peroxynitrite (k = 1×10^6 M^{-1} s^{-1})	*Mt*TrxB, *Mt*TrxC	Herein
PrxQ (Rv2125)	PrxQ/Bcp	ND	ND	–

[a] Value determined for *Salmonella typhimurium* AhpC. MtAhpC reduced H2O2 faster than *t*-bOOH, Cumene-OOH and linoleic acid-derived hydroperoxides, but the precise rate constant value for the reaction was not reported [30]. MtAhpD is *M. tuberculosis* alkyl hydroperoxide reductase D and MtMrx 1 is *M. tuberculosis* mycoredoxin 1. Reactivities with peroxynitrite are apparent rate constants at physiological pH, except for AhpC (pH 6.8).
[b] After long incubation times, mycothiol alone could also reduce oxidized *Mt*AhpE, but the importance of this reaction under catalytic conditions was not determined [78].

replaced by a basic amino acid (Arg) in *Mt*PrxQ B sequence, which is largely responsible for the loss in hydrophobicity and symmetry in the corresponding surface of *Mt*PrxQ B (Fig. S5 a)) when compared to the interface surface of dimeric PrxQs as illustrated below for *Ap*PrxQ (Fig. S5 b)).

Our results showed that oxidized *Mt*PrxQ B is also monomeric (Fig. 6). Both the secondary and tertiary structure of *Mt*PrxQ B are influenced by the redox state of the protein (Fig. 7a) and b)). Data is compatible with a partial unfolding of the α2 helix previously reported to occur during FF to LU transition in other members of the subfamily [10]. In addition, *Mt*PrxQ B oxidation determined an important distortion of the microenvironment surrounding both Cys, which was accompanied by conformational rotations in the side-chain of a series of aromatic residues in the proximity of the active site, which led to an important solvent exposure increase (Fig. 8). Further work is required to establish whether the kinetics of the conformational transition between the FF and LU forms of *Mt*PrxQ B reported herein is compatible with the kinetics of its catalytic cycle.

In conclusion, *Mt*PrxQ B shows high catalytic efficiency towards the reduction of FA-OOH using homologous *Mt*Trx B and C as reductants. The protein secondary and tertiary structure is affected upon oxidation, and particularly several hydrophobic residues get exposed in the oxidized enzyme, which otherwise remains monomeric both under reduced and oxidized state. *Mt*PrxQ B has been reported to be essential for *M. tuberculosis* growth in media containing cholesterol as the principal carbon source, which is an essential nutrient during animal chronic infections [16]. A tempting explanation was that *Mt*PrxQ B reduced cholesterol-OOH. However, our data indicate that the enzyme lacked activity on that substrate. Since cholesterol metabolism affects mycobacterial lipid composition [71,72], other possibility is that *Mt*PrxQ B could reduce hydoperoxides derived from other mycobacterial lipids preferentially synthesized when grown on cholesterol. Further work should asses the relationship between *Mt*PrxQ B essentiality and its lipid hydroperoxidase activity.

Funding

This work was supported by grants from Universidad de la República (CSIC Grupos 767 and Espacio Interdisciplinario), CONICET (PIP-11220110100723), ANPCyT (PICT2014-1022 and PICT2013-0982) and UBACyT (20020130100097BA and 20020130100468BA). A. M. Reyes was partially supported by a PhD scholarship from Universidad de la República-CAP, Uruguay and D.S. Vazquez was supported by a PhD scholarship from Universidad de Buenos Aires, Argentina.

Acknowledgements

We thank Dr. Balaraman Kalyanaraman from the Medical College of Wisconsin, Milwaukee, USA, for kindly providing the CBA. We also thank Dr. Ahmed Haouz from Institut Pasteur Paris, Dr. Marcelo Comini from Institut Pasteur Montevideo and Dr. Leopold Flohé, from Universidad de la República, Uruguay and University of Padova, Italy, for providing the plasmids for the expression of the recombinant proteins used herein as described under Materials section.

Appendix A. Supporting information

Supplementary data associated with this article can be found in the online version at doi:10.1016/j.freeradbiomed.2016.10.005.

References

[1] E. Leibert, M. Danckers, W.N. Rom, New drugs to treat multidrug-resistant tuberculosis: the case for bedaquiline, Ther. Clin. Risk Manag. 10 (2014) 597–602.
[2] C. Nathan, M.U. Shiloh, Reactive oxygen and nitrogen intermediates in the relationship between mammalian hosts and microbial pathogens, Proc. Natl. Acad. Sci. USA 97 (2000) 8841–8848.
[3] M.U. Shiloh, C.F. Nathan, Reactive nitrogen intermediates and the pathogenesis of Salmonella and mycobacteria, Curr. Opin. Microbiol. 3 (2000) 35–42.
[4] M., R.R. Hugo, M. Trujillo, Thiol-dependent peroxidases in Mycobacterium tuberculosis antioxidant defense, in: P.-J. Cardona (Ed.)Understanding Tuberculosis – Deciphering the Secret Life of the Bacilli, InTech, Croatia, 2011, pp. 293–316.
[5] M.N. Alvarez, G. Peluffo, L. Piacenza, R. Radi, Intraphagosomal peroxynitrite as a macrophage-derived cytotoxin against internalized Trypanosoma cruzi: consequences for oxidative killing and role of microbial peroxiredoxins in infectivity, J. Biol. Chem. 286 (2011) 6627–6640.
[6] S.T. Cole, B.G. Barrell, Analysis of the genome of Mycobacterium tuberculosis H37Rv, Novartis Found. Symp. 217 (1998) 160–172 (discussion 172-167).
[7] S.G. Rhee, H.A. Woo, I.S. Kil, S.H. Bae, Peroxiredoxin functions as a peroxidase and a regulator and sensor of local peroxides, J. Biol. Chem. 287 (2012) 4403–4410.
[8] M. Trujillo, G. Ferrer-Sueta, L. Thomson, L. Flohe, R. Radi, Kinetics of peroxiredoxins and their role in the decomposition of peroxynitrite, Subcell. Biochem. 44 (2007) 83–113.
[9] J.M. Lew, A. Kapopoulou, L.M. Jones, S.T. Cole, TubercuList--10 years after, Tuberculosis 91 (2011) 1–7.
[10] A. Perkins, M.C. Gretes, K.J. Nelson, L.B. Poole, P.A. Karplus, Mapping the active site helix-to-strand conversion of CxxxxC peroxiredoxin Q enzymes, Biochemistry 51 (2012) 7638–7650.
[11] S. Gu, J. Chen, K.M. Dobos, E.M. Bradbury, J.T. Belisle, X. Chen, Comprehensive proteomic profiling of the membrane constituents of a Mycobacterium tuberculosis strain, Mol. Cell Proteom. 2 (2003) 1284–1296.
[12] K.G. Mawuenyega, C.V. Forst, K.M. Dobos, J.T. Belisle, J. Chen, E.M. Bradbury, A.R. Bradbury, X. Chen, Mycobacterium tuberculosis functional network analysis by global subcellular protein profiling, Mol. Biol. Cell 16 (2005) 396–404.
[13] H. Malen, S. Pathak, T. Softeland, G.A. de Souza, H.G. Wiker, Definition of novel cell envelope associated proteins in Triton X-114 extracts of Mycobacterium tuberculosis H37Rv, BMC Microbiol. 10 (2010) 132.
[14] G.A. de Souza, M.O. Arntzen, S. Fortuin, A.C. Schurch, H. Malen, C.R. McEvoy, D. van Soolingen, B. Thiede, R.M. Warren, H.G. Wiker, Proteogenomic analysis of polymorphisms and gene annotation divergences in prokaryotes using a clustered mass spectrometry-friendly database, Mol. Cell Proteom. 10 (M110) (2011) 002527.
[15] J.E. Griffin, J.D. Gawronski, M.A. Dejesus, T.R. Ioerger, B.J. Akerley, C.M. Sassetti, High-resolution phenotypic profiling defines genes essential for mycobacterial growth and cholesterol catabolism, PLoS Pathog. 7 (2011) e1002251.
[16] R. Van der Geize, K. Yam, T. Heuser, M.H. Wilbrink, H. Hara, M.C. Anderton, E. Sim, L. Dijkhuizen, J.E. Davies, W.W. Mohn, L.D. Eltis, A gene cluster encoding cholesterol catabolism in a soil actinomycete provides insight into Mycobacterium tuberculosis survival in macrophages, Proc. Natl. Acad. Sci. USA 104 (2007)

1947–1952.
[17] L.B. Poole, The catalytic mechanism of peroxiredoxins, Subcell. Biochem. 44 (2007) 61–81.
[18] D.J. Clarke, X.P. Ortega, C.L. Mackay, M.A. Valvano, J.R. Govan, D.J. Campopiano, P. Langridge-Smith, A.R. Brown, Subdivision of the bacterioferritin comigratory protein family of bacterial peroxiredoxins based on catalytic activity, Biochemistry 49 (2010) 1319–1330.
[19] B.B. Horta, M.A. de Oliveira, K.F. Discola, J.R. Cussiol, L.E. Netto, Structural and biochemical characterization of peroxiredoxin Qbeta from Xylella fastidiosa: catalytic mechanism and high reactivity, J. Biol. Chem. 285 (2010) 16051–16065.
[20] N. Rouhier, E. Gelhaye, J.M. Gualberto, M.N. Jordy, E. De Fay, M. Hirasawa, S. Duplessis, S.D. Lemaire, P. Frey, F. Martin, W. Manieri, D.B. Knaff, J.P. Jacquot, Poplar peroxiredoxin Q. A thioredoxin-linked chloroplast antioxidant functional in pathogen defense, Plant Physiol. 134 (2004) 1027–1038.
[21] S.A. Reeves, D. Parsonage, K.J. Nelson, L.B. Poole, Kinetic and thermodynamic features reveal that Escherichia coli BCP is an unusually versatile peroxiredoxin, Biochemistry 50 (2011) 8970–8981.
[22] M.K. Cha, S.K. Hong, I.H. Kim, Four thiol peroxidases contain a conserved GCT catalytic motif and act as a versatile array of lipid peroxidases in Anabaena sp. PCC7120, Free Radic. Biol. Med. 42 (2007) 1736–1748.
[23] G. Wang, A.A. Olczak, J.P. Walton, R.J. Maier, Contribution of the Helicobacter pylori thiol peroxidase bacterioferritin comigratory protein to oxidative stress resistance and host colonization, Infect. Immun. 73 (2005) 378–384.
[24] W. Jeong, M.K. Cha, I.H. Kim, Thioredoxin-dependent hydroperoxide peroxidase activity of bacterioferritin comigratory protein (BCP) as a new member of the thiol-specific antioxidant protein (TSA)/Alkyl hydroperoxide peroxidase C (AhpC) family, J. Biol. Chem. 275 (2000) 2924–2930.
[25] J. Zielonka, A. Sikora, J. Joseph, B. Kalyanaraman, Peroxynitrite is the major species formed from different flux ratios of co-generated nitric oxide and superoxide: direct reaction with boronate-based fluorescent probe, J. Biol. Chem. 285 (2010) 14210–14216.
[26] J.S. Beckman, T.W. Beckman, J. Chen, P.A. Marshall, B.A. Freeman, Apparent hydroxyl radical production by peroxynitrite: implications for endothelial injury from nitric oxide and superoxide, Proc. Natl. Acad. Sci. USA 87 (1990) 1620–1624.
[27] R. Radi, J.S. Beckman, K.M. Bush, B.A. Freeman, Peroxynitrite oxidation of sulfhydryls. The cytotoxic potential of superoxide and nitric oxide, J. Biol. Chem. 266 (1991) 4244–4250.
[28] B. Alvarez, V. Demicheli, R. Duran, M. Trujillo, C. Cervenansky, B.A. Freeman, R. Radi, Inactivation of human Cu,Zn superoxide dismutase by peroxynitrite and formation of histidinyl radical, Free Radic. Biol. Med. 37 (2004) 813–822.
[29] S. Mitra, S.R. Dungan, Cholesterol solubilization in aqueous micellar solutions of quillaja saponin, bile salts, or nonionic surfactants, J. Agric. Food Chem. 49 (2001) 384–394.
[30] T. Jaeger, H. Budde, L. Flohe, U. Menge, M. Singh, M. Trujillo, R. Radi, Multiple thioredoxin-mediated routes to detoxify hydroperoxides in Mycobacterium tuberculosis, Arch. Biochem. Biophys. 423 (2004) 182–191.
[31] A. Claiborne, H. Miller, D. Parsonage, R.P. Ross, Protein-sulfenic acid stabilization and function in enzyme catalysis and gene regulation, FASEB J. 7 (1993) 1483–1490.
[32] H. Yin, N.A. Porter, Specificity of the ferrous oxidation of xylenol orange assay: analysis of autoxidation products of cholesteryl arachidonate, Anal. Biochem. 313 (2003) 319–326.
[33] C.N. Pace, F. Vajdos, L. Fee, G. Grimsley, T. Gray, How to measure and predict the molar absorption coefficient of a protein, Protein Sci. 4 (1995) 2411–2423.
[34] G.L. Ellman, Tissue sulfhydryl groups, Arch. Biochem. Biophys. 82 (1959) 70–77.
[35] G.R. Schonbaum, S. Lo, Interaction of peroxidases with aromatic peracids and alkyl peroxides. Product analysis, J. Biol. Chem. 247 (1972) 3353–3360.
[36] A. Holmgren, Thioredoxin structure and mechanism: conformational changes on oxidation of the active-site sulfhydryls to a disulfide, Structure 3 (1995) 239–243.
[37] M. Trujillo, P. Mauri, L. Benazzi, M. Comini, A. De Palma, L. Flohe, R. Radi, M. Stehr, M. Singh, F. Ursini, T. Jaeger, The mycobacterial thioredoxin peroxidase can act as a one-cysteine peroxiredoxin, J. Biol. Chem. 281 (2006) 20555–20566.
[38] A.M. Reyes, M. Hugo, A. Trostchansky, L. Capece, R. Radi, M. Trujillo, Oxidizing substrate specificity of Mycobacterium tuberculosis alkyl hydroperoxide reductase E: kinetics and mechanisms of oxidation and overoxidation, Free Radic. Biol. Med. 51 (2011) 464–473.
[39] R. Bou, R. Codony, A. Tres, E.A. Decker, F. Guardiola, Determination of hydroperoxides in foods and biological samples by the ferrous oxidation-xylenol orange method: a review of the factors that influence the method's performance, Anal. Biochem. 377 (2008) 1–15.
[40] K.J. Nelson, D. Parsonage, Measurement of peroxiredoxin activity, Curr. Protoc. Toxicol. (2011) Chapter 7, Unit7 10.
[41] B.A. Sermon, J.F. Eccleston, R.H. Skinner, P.N. Lowe, Mechanism of inhibition by arachidonic acid of the catalytic activity of Ras GTPase-activating proteins, J. Biol. Chem. 271 (1996) 1566–1572.
[42] K. Dalziel, Initial stady state velocities in the evaluation of enzyme-substrate reaction mechanisms, Acta Chem. Scand. 11 (1957) 1706–1723.
[43] R. Radi, Kinetic analysis of reactivity of peroxynitrite with biomolecules, Methods Enzymol. 269 (1996) 354–366.
[44] M. Trujillo, G. Ferrer-Sueta, R. Radi, Kinetic studies on peroxynitrite reduction by peroxiredoxins, Methods Enzymol. 441 (2008) 173–196.
[45] R. Ogusucu, D. Rettori, D.C. Munhoz, L.E. Netto, O. Augusto, Reactions of yeast thioredoxin peroxidases I and II with hydrogen peroxide and peroxynitrite: rate constants by competitive kinetics, Free Radic. Biol. Med. 42 (2007) 326–334.
[46] Y. Hayashi, I. Yamazaki, The oxidation-reduction potentials of compound I/compound II and compound II/ferric couples of horseradish peroxidases A2 and C, J. Biol. Chem. 254 (1979) 9101–9106.
[47] R. Floris, S.R. Piersma, G. Yang, P. Jones, R. Wever, Interaction of myeloperoxidase with peroxynitrite. A comparison with lactoperoxidase, horseradish peroxidase and catalase, Eur. J. Biochem. 215 (1993) 767–775.
[48] B. Manta, M. Hugo, C. Ortiz, G. Ferrer-Sueta, M. Trujillo, A. Denicola, The peroxidase and peroxynitrite reductase activity of human erythrocyte peroxiredoxin 2, Arch. Biochem. Biophys. 484 (2009) 146–154.
[49] M. Hugo, L. Turell, B. Manta, H. Botti, G. Monteiro, L.E. Netto, B. Alvarez, R. Radi, M. Trujillo, Thiol and sulfenic acid oxidation of AhpE, the one-cysteine peroxiredoxin from Mycobacterium tuberculosis: kinetics, acidity constants, and conformational dynamics, Biochemistry 48 (2009) 9416–9426.
[50] V. Demicheli, D.M. Moreno, G.E. Jara, A. Lima, S. Carballal, N. Rios, C. Batthyany, G. Ferrer-Sueta, C. Quijano, D.A. Estrin, M.A. Marti, R. Radi, Mechanism of the reaction of human manganese superoxide dismutase with peroxynitrite: nitrationnitration of critical tyrosine 34, Biochemistry 55 (2016) 3403–3417.
[51] A. Perkins, L.B. Poole, P.A. Karplus, Tuning of peroxiredoxin catalysis for various physiological roles, Biochemistry 53 (2014) 7693–7705.
[52] K. Arnold, L. Bordoli, J. Kopp, T. Schwede, The SWISS-MODEL workspace: a web-based environment for protein structure homology modelling, Bioinformatics 22 (2006) 195–201.
[53] W.L. Jorgensen, J. Chandrasekhar, J.D. Madura, R.W. Impey, M.L. Klein, Comparison of simple potential functions for simulating liquid water, J. Chem. Phys. 79 (1983) 926–935.
[54] D.A. Pearlman, D.A. Case, J.W. Caldwell, W.S. Ross, T.E. Cheatham, S. DeBolt, D. Ferguson, G. Seibel, P. Kollman, AMBER, a package of computer programs for applying molecular mechanics, normal mode analysis, molecular dynamics and free energy calculations to simulate the structural and energetic properties of molecules, Comput. Phys. Commun. 91 (1995) 1–41.
[55] W. Humphrey, A. Dalke, K. Schulten, VMD: visual molecular dynamics, J. Mol. Graph. 14 (33–38) (1996) 27–38.
[56] R. Goldman, D.A. Stoyanovsky, B.W. Day, V.E. Kagan, Reduction of phenoxyl radicals by thioredoxin results in selective oxidation of its SH-groups to disulfides. An antioxidant function of thioredoxin, Biochemistry 34 (1995) 4765–4772.
[57] D.J. Clarke, C.L. Mackay, D.J. Campopiano, P. Langridge-Smith, A.R. Brown, Interrogating the molecular details of the peroxiredoxin activity of the Escherichia coli bacterioferritin comigratory protein using high-resolution mass spectrometry, Biochemistry 48 (2009) 3904–3914.
[58] S.J. Liao, C.Y. Yang, K.H. Chin, A.H. Wang, S.H. Chou, Insights into the alkyl peroxide reduction pathway of Xanthomonas campestris bacterioferritin comigratory protein from the trapped intermediate-ligand complex structures, J. Mol. Biol. 390 (2009) 951–966.
[59] M. Wakita, S. Masuda, K. Motohashi, T. Hisabori, H. Ohta, K. Takamiya, The significance of type II and PrxQ peroxiredoxins for antioxidative stress response in the purple bacterium Rhodobacter sphaeroides, J. Biol. Chem. 282 (2007) 27792–27801.
[60] D. Limauro, E. Pedone, I. Galdi, S. Bartolucci, Peroxiredoxins as cellular guardians in Sulfolobus solfataricus: characterization of Bcp1, Bcp3 and Bcp4, FEBS J. 275 (2008) 2067–2077.
[61] D. Dolman, G.A. Newell, M.D. Thurlow, A kinetic study of the reaction of horseradish peroxidase with hydrogen peroxide, Can. J. Biochem. 53 (1975) 495–501.
[62] W.H. Koppenol, J.J. Moreno, W.A. Pryor, H. Ischiropoulos, J.S. Beckman, Peroxynitrite, a cloaked oxidant formed by nitric oxide and superoxide, Chem. Res. Toxicol. 5 (1992) 834–842.
[63] Z.A. Wood, L.B. Poole, R.R. Hantgan, P.A. Karplus, Dimers to doughnuts: redox-sensitive oligomerization of 2-cysteine peroxiredoxins, Biochemistry 41 (2002) 5493–5504.
[64] A. Rath, A.R. Davidson, C.M. Deber, The structure of "unstructured" regions in peptides and proteins: role of the polyproline II helix in protein folding and recognition, Biopolymers 80 (2005) 179–185.
[65] A. Perkins, D. Parsonage, K.J. Nelson, O.M. Ogba, P.H. Cheong, L.B. Poole, P.A. Karplus, Peroxiredoxin catalysis at atomic resolution, Structure 24 (2016) 1668–1678.
[66] S. Mongkolsuk, W. Praituan, S. Loprasert, M. Fuangthong, S. Chamnongpol, Identification and characterization of a new organic hydroperoxide resistance (ohr) gene with a novel pattern of oxidative stress regulation from Xanthomonas campestris pv. phaseoli, J. Bacteriol. 180 (1998) 2636–2643.
[67] M. Si, J. Wang, X. Xiao, J. Guan, Y. Zhang, W. Ding, M.T. Chaudhry, Y. Wang, X. Shen, Ohr protects Corynebacterium glutamicum against organic hydroperoxide induced oxidative stress, PLoS One 10 (2015) e0131634.
[68] A. Zeida, A.M. Reyes, P. Lichtig, M. Hugo, D.S. Vazquez, J. Santos, F.L. Gonzalez Flecha, R. Radi, D.A. Estrin, M. Trujillo, Molecular basis of hydroperoxide specificity in peroxiredoxins: the case of AhpE from Mycobacterium tuberculosis, Biochemistry 54 (2015) 7237–7247.
[69] E. Pedone, D. Limauro, R. D'Alterio, M. Rossi, S. Bartolucci, Characterization of a multifunctional protein disulfide oxidoreductase from Sulfolobus solfataricus, FEBS J. 273 (2006) 5407–5420.
[70] E. Pedone, D. Limauro, S. Bartolucci, The machinery for oxidative protein folding in thermophiles, Antioxid. Redox Signal. 10 (2008) 157–169.
[71] M. Jain, C.J. Petzold, M.W. Schelle, M.D. Leavell, J.D. Mougous, C.R. Bertozzi, J.A. Leary, J.S. Cox, Lipidomics reveals control of Mycobacterium tuberculosis virulence lipids via metabolic coupling, Proc. Natl. Acad. Sci. USA 104 (2007) 5133–5138.
[72] J.E. Griffin, A.K. Pandey, S.A. Gilmore, V. Mizrahi, J.D. McKinney, C.R. Bertozzi, C.M. Sassetti, Cholesterol catabolism by Mycobacterium tuberculosis requires transcriptional and metabolic adaptations, Chem. Biol. 19 (2012) 218–227.

[73] P. Lamkemeyer, M. Laxa, V. Collin, W. Li, I. Finkemeier, M.A. Schottler, V. Holtkamp, V.B. Tognetti, E. Issakidis-Bourguet, A. Kandlbinder, E. Weis, M. Miginiac-Maslow, K.J. Dietz, Peroxiredoxin Q of Arabidopsis thaliana is attached to the thylakoids and functions in context of photosynthesis, Plant J. 45 (2006) 968–981.
[74] D. Parsonage, P.A. Karplus, L.B. Poole, Substrate specificity and redox potential of AhpC, a bacterial peroxiredoxin, Proc. Natl. Acad. Sci. USA 105 (2008) 8209–8214.
[75] R. Bryk, P. Griffin, C. Nathan, Peroxynitrite reductase activity of bacterial peroxiredoxins, Nature 407 (2000) 211–215.
[76] R. Bryk, C.D. Lima, H. Erdjument-Bromage, P. Tempst, C. Nathan, Metabolic enzymes of mycobacteria linked to antioxidant defense by a thioredoxin-like protein, Science 295 (2002) 1073–1077.
[77] M. Hugo, K. Van Laer, A.M. Reyes, D. Vertommen, J. Messens, R. Radi, M. Trujillo, Mycothiol/mycoredoxin 1-dependent reduction of the peroxiredoxin AhpE from Mycobacterium tuberculosis, J. Biol. Chem. 289 (2014) 5228–5239.
[78] A. Kumar, A.M. Balakrishna, W. Nartey, M.S. Manimekalai, G. Gruber, Redox chemistry of Mycobacterium tuberculosis alkylhydroperoxide reductase E (AhpE): structural and mechanistic insight into a mycoredoxin-1 independent reductive pathway of AhpE via mycothiol, Free Radic. Biol. Med. 97 (2016) 588–601.
[79] P. Mendes, GEPASI: a software package for modelling the dynamics, steady states and control of biochemical and other systems, Comput. Appl. Biosci. 9 (1993) 563–571.